Available online at www.sciencedirect.com
ScienceDirect
Polymer 48 (2007) 4123–4129
polymer
www.elsevier.com/locate/polymer

Polymethylene-*block*-poly(dimethyl siloxane)-*block*-polymethylene nanoaggregates in toluene at room temperature

Jiandong Wang [a], J. Hugh Horton [a], Guojun Liu [a,*], Sun-Yeol Lee [b], Kenneth J. Shea [b]

[a] *Department of Chemistry, Queen's University, 90 Bader Lane, Kingston, Ontario, Canada K7L 3N6*
[b] *Department of Chemistry, University of California, Irvine, 5042B Frederick Reines Hall, Irvine, CA 92697-4575, USA*

Received 6 March 2007; received in revised form 28 April 2007; accepted 4 May 2007
Available online 18 May 2007

Abstract

Aggregates of a polymethylene-*block*-poly(dimethyl siloxane)-*block*-polymethylene (PM-PDMS-PM) sample were prepared in toluene by cooling down a toluene solution of the sample slowly from 105 °C to room temperature. Atomic force microscopic (AFM) and electron microscopic (EM) studies revealed that the aggregates included triblock crystal plates with sizes of upto tens of micrometers and PM-PDMS-PM nanodiscs. Surprisingly and interestingly, we discovered that the topographic images of the nanodiscs obtained by tapping-mode AFM changed from nanodiscs at light tapping to strikingly beautiful nanodonuts at moderate tapping and then filled nanodonuts at heavy tapping. Justification for such observations is provided.

Keywords: Block copolymers; Atom force microscopy; Morphologies of micelles

1. Introduction

Aggregation and micellization (only if the aggregates formed are thermodynamic products) of block copolymers in block-selective solvents yield nanoparticles with shapes ranging from spheres [1,2] to cylinders [3–5], tubes [6–10], vesicles [4,5,11–14], donuts [5,15,16], and many others [17]. The shape diversity of such aggregates may help their applications in nanofabrication [18–20], lithography [21–23], cell culturing [24,25], and drug delivery [26,27]. While unusual micelles (with shapes that differ from spheres) can be prepared from coil–coil amorphous block copolymers, they may be more readily prepared from copolymers containing crystallizable blocks, because the crystallization of one block or the regular parallel packing of chains of a block promotes low-curvature core–corona interfaces and thus favors the formation of cylinders, nanotubes, and vesicles [28,29]. This rule seems to be supported also by the ready formation of vesicles [11,30] and mushroom-like structures [31] from rod–coil diblock copolymers, where the rod block prefers parallel packing. It was for potential discovery of new morphologies we initiated the study of aggregates of polymethylene-*block*-poly(dimethyl siloxane)-*block*-polymethylene (PM-PDMS-PM) where the PM blocks are crystalline and are insoluble in most solvents at room temperature. While past studies on block copolymers containing crystalline polyethylene [31,32] (PE) or poly(ethylene oxide) [33,34] (PEO) block(s) have mostly dealt with large plate-like crystals with sizes >1 μm, we focus our attention here on PM nanodiscs covered by PDMS loops. We show that electron microscopy, which has been the most popular technique in establishing morphologies of block copolymer nanoaggregates and micelles, did beam damage to the nanodiscs, whereas tapping-mode AFM is effective in imaging these structures after the nanodiscs are aspirated on mica surfaces from toluene. We show further the intriguing changes in the height and phase images of these nanodiscs with tapping force and present explanations for the

* Corresponding author.
E-mail address: guojun.liu@chem.queensu.ca (G. Liu).

0032-3861/$ - see front matter
doi:10.1016/j.polymer.2007.05.029

observed phenomena, which should be of value to future AFM users.

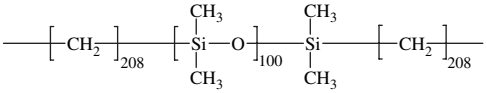

2. Experimental section

2.1. Aggregate preparation

Our visual observation revealed that the triblock dissolved in toluene between 85 and 90 °C, which should be close to the melting temperatures T_m of the PM blocks. Complete dissolution of the triblock was ensured by stirring it in toluene at 105 °C for 4.5 h. For aggregate formation, the toluene samples immersed in an oil bath with a total volume of 1 L were allowed to cool to room temperature in a fume hood on a hotplate spontaneously. Our observation indicated that the time taken for the oil bath to cool from 105 to 60 °C was 25 min and another 50 min elapsed before the oil cooled to 40 °C. Such mixtures were examined only after they had been equilibrated at room temperature for at least 12 h. The triblock concentration used was always between 1.6 and 2.0 mg/mL.

2.2. Electron microscopic studies

For transmission electron microscopic (TEM) studies, the triblock aggregate solutions in toluene were aspirated on carbon-coated copper grids before examination by a Hitachi-7000 microscope. The operating voltage used was 75 kV. Scanning electron microscopic (SEM) images were acquired on a Microlab 310-F surface analysis system (Thermo/VG Scientific, Hastings, UK) using 15 kV beam energy and 2 nA sample current. The polymer particles were aspirated on a mica substrate coated by a 6-nm thick gold layer before examination.

2.3. AFM measurements

For AFM measurements, the aggregate solutions were centrifuged at 1550 *g* before aspiration onto surfaces of freshly cleaved mica. The images were obtained on a Veeco multimode microscope equipped with a Nanoscope IIIa controller operating in the tapping mode. The tips used were of model RTESP7 of the Veeco NanoProbeTM type with resonance frequency ~300 kHz and a radius of curvature typically less than 5 nm. The tip oscillation amplitude A_0 in air was ~45 nm for all images presented.

3. Results and discussion

3.1. Polymer synthesis and characterization

The details for the synthesis of the triblock have been reported before [35]. It involved hydroboration of α,ω-divinylpoly(dimethyl siloxane) by thexylborane. The soluble borane produced then functioned as an initiator to react with dimethylsulfoxonium methylide by homologation to produce the PM chains. The polymerization was terminated by de-activating the borane centers using an aqueous sodium hydroxide and hydrogen peroxide mixture. The α,ω-divinylpoly(dimethyl siloxane) precursor was provided by General Electric Corp. that possessed a low polydispersity and 100 units. The number of methylene units *n* per PM was determined from ^{1}H NMR analysis in deuterated toluene at 90 °C to be 208. At this *n* value, the weight fraction of the PM in the sample is 44%. The polydispersity of the samples in terms of their weight- to number-average molar mass ratio M_w/M_n was determined in xylene at 90 °C to be 1.04 based on polyethylene standards.

3.2. Overview of the aggregates formed

Solutions of the triblock in toluene at room temperature were prepared by heating the triblock in toluene at 105 °C for 4.5 h and then cooling the samples slowly. After equilibrating at room temperature overnight, the solutions consisted of a supernatant that bore a visible bluish tint and a precipitate at the bottom.

To gain an overview of the aggregates present, we vigorously shook the toluene solution to suspend the precipitate before its aspiration onto a carbon-coated copper grid for analysis by TEM. Fig. 1 shows a TEM image of the sample. The plate-like structures correspond to PM-PDMS-PM crystals.

We also checked by TEM the morphologies of the aggregates left in the supernatant. The concentration of large crystal plates in the supernatant obviously decreased as judged by the increased difficulty in finding them by TEM. Aside from the occasional observation of crystal plates, we noticed the presence of many nanoparticles that were unstable and ''melted'' immediately in the electron beam, despite the fact that we intentionally reduced the beam intensity. Due to the instability

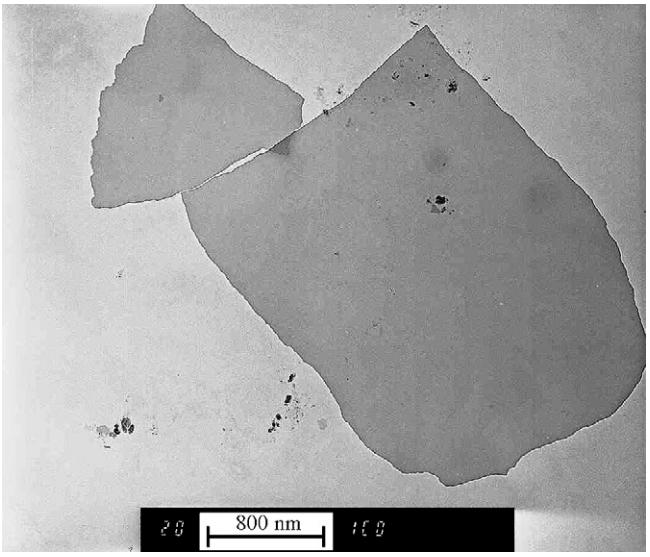

Fig. 1. TEM image of two PM-PDMS-PM crystal plates.

of the nanoaggregates in electron beams, we then examined these structures by AFM. Fig. 2a shows a topographic image of a sample measured by AFM at a set point amplitude ratio r_{SP} or A/A_0 of 0.75, where A denotes the oscillating amplitude of a tip interacting with a sample and r_{SP} decreases with increasing tapping force. Particles of different sizes are observed. By far the most dominant species in the images were uniform circular structures with a dark core and bright circular periphery. If the traditional AFM image interpretation rule of ''being dark means low'' applies, this suggests the presence of ''donut-like'' nanoaggregates in the system, structures that are rarely seen in block copolymer systems with formation mechanism still not well understood [5,16,36].

While TEM could not be used to examine the structure of the nanoaggregates, we were more fortunate with an SEM system. In this case, we noticed that image degradation became obvious within about 30 s of scanning a 1 μm × 1 μm area. To minimize beam damage, we focused on one region of a sample and then moved to a pristine area without further focusing to obtain an image within 2–3 s. This yielded us some images but limited our ability to focus well. Fig. 2b shows such an image with poor focus. Despite the focus, it does indicate that the sample contained circular particles with a diameter of ~60 nm. While the size of these circular objects is consistent with that obtained by AFM for the ''nanodonuts'', the annular shape is not seen in the SEM image. The image also shows the presence of larger particles and particles of other shapes again in agreement with AFM observations.

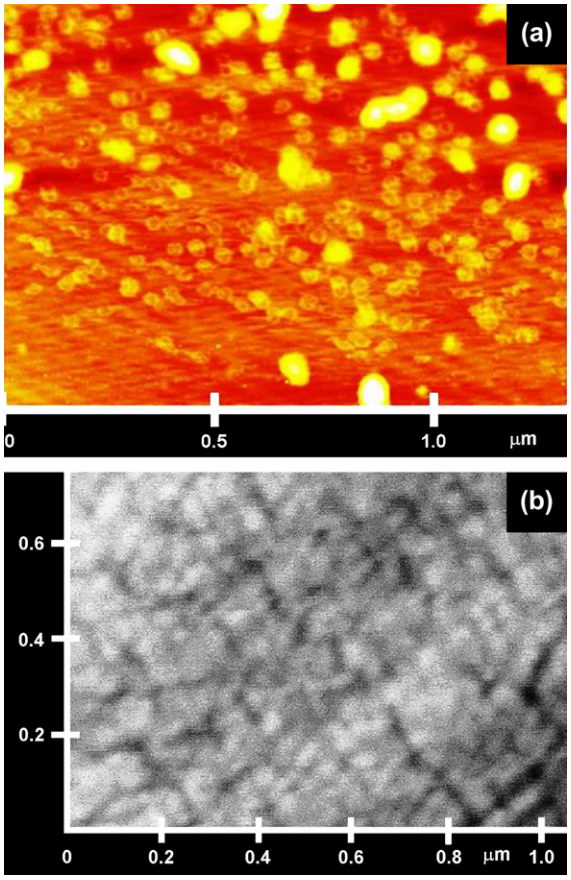

Fig. 2. Topographic AFM image (a) and SEM image (b) of nanoaggregates of PM-PDMS-PM aspirated from toluene on mica and Au-coated mica.

3.3. Crystal plates

The study of crystallization of a crystalline block or blocks of block copolymers has received much attention over the past few decades. PE and poly(ethylene oxide) (PEO) have been the favorable crystalline blocks used. Many of the studies dealt with phase segregation of PE and PEO-containing block copolymers in bulk. Such systems were examined to shed light on confinement effects on polymer crystallization [37,38]. When crystallization of PE or PEO-containing block copolymers from dilute solution was studied, microscopic [33,34,39] and scattering [31,32] studies confirmed that the PE and PEO blocks formed square crystalline plates with thickness between ~5 and ~20 nm. Thus, observation of PM-PDMS-PM crystal plates here is not surprising but in agreement with prior reports.

3.4. Nanoaggregates

While a more detailed study of crystallization of PM-PDMS-PM can be interesting, we focused on the structural elucidation of the ''donut-like'' nanoaggregates for their ''novelty''. Fig. 3 compares the topographic and phase images of the nanoaggregate structures at the r_{SP} values of 0.95, 0.75, and 0.60. The nanoaggregates have a ''donut-like'' structure at $r_{SP} = 0.75$ in the topographic image, consisting of a dark core and bright periphery. At $r_{SP} = 0.60$ the contrast is reversed and the nanoaggregates now appear to have a ''filled donut'' structure with a brighter core and darker periphery. Finally, at $r_{SP} = 0.95$ the annular structure can no longer be discerned, and the nanoaggregates appear in the topographic images as ''circular objects''. We also notice that the phase contrast between the core and shell increased as r_{SP} decreased. The overall apparent size of the core–shell particles increased from 49 ± 12 to 68 ± 17 and 97 ± 24 nm as r_{SP} decreased from 0.95 to 0.75 and 0.60.

The fact that the topographic images changed with r_{SP} surprised us initially. Despite the complication, we know that the structures obtained at $r_{SP} = 0.95$ would be the closest to the true ones for the minimal tapping force used [40]. For this, we will examine closely in this subsection the images obtained at $r_{SP} = 0.95$.

A closer analysis of the particles in Fig. 3a at $r_{SP} = 0.95$ using the Veeco image analysis software Particle Analysis, we obtained for the particles an average height h of 2.7 ± 1.1 nm and an average diameter d of 49 ± 12 nm. While the actual diameter can be slightly off for the finite radius of curvature of 5 nm for the tip, this does not detract one from the fact that the thickness to diameter ratio is very small. Based on the small thickness to diameter ratio, we conclude that the ''circular objects'' are nanodiscs or nanoplates. The fact that a core–shell structure is revealed in both the topographic and phase images at $r_{SP} = 0.75$ and $r_{SP} = 0.60$

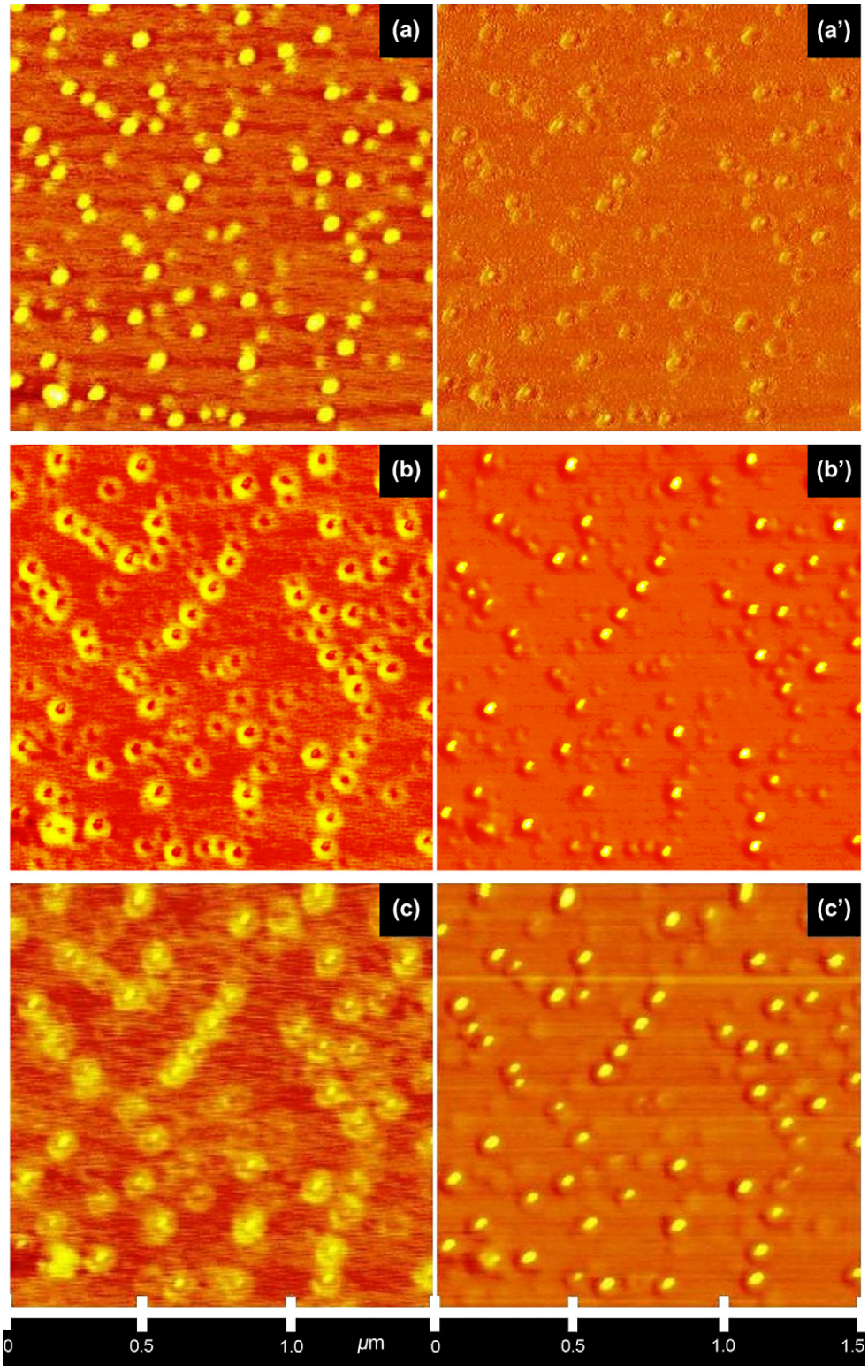

Fig. 3. Topographic (left) and phase (right) AFM images of PM-PDMS-PM nanoaggregates aspirated on mica from toluene. The A_0 value used for AFM imaging was always ~45 nm. The r_{SP} values used were 0.95 (top), 0.75 (middle), and 0.60 (bottom).

suggests that the nanodiscs must contain both PM and PDMS. Since PM is insoluble in toluene and PDMS is soluble at room temperature, PM should form the core of the particles and PDMS should form the shell as schematically illustrated in Fig. 4. To further hypothesize chain packing inside the PM and PDMS domains, we make use of the fact that PM crystallizes and favors parallel chain packing. Our assumption is, therefore, that the nanodiscs may bear structural resemblance to the larger crystal plates with chain packing illustrated in Fig. 4b when dispersed in toluene.

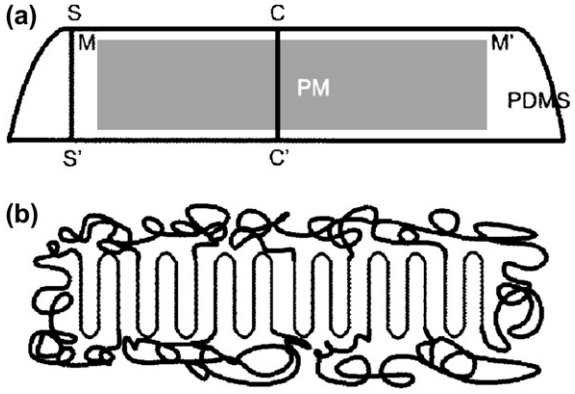

Fig. 4. Schematic illustration of domain structures in PM-PDMS-PM nanodiscs deposited on mica surfaces (top) and possible chain packing in such nanodiscs in toluene (bottom).

The PE crystal plates or crystals of block copolymers containing a PE block formed at a given temperature normally possesses a certain thickness or a narrow distribution [31,41]. The nanodiscs in Fig. 3a have thickness of 2.7 ± 1.1 nm, which represents quite a wide range of thickness variation. While one can argue for the formation of the nanodiscs at different temperatures, we tend to believe that the nanodiscs are kinetic rather than thermodynamic products, because the relative population of the nanodiscs at room temperature in toluene depended on how a sample was cooled. When toluene was cooled by the protocol stated in Section 2, we obtained a supernatant with a light bluish tint and much precipitate. The precipitate content was minimal when we quickly quenched a hot PM-PDMS-PM solution in toluene into room temperature water. More nanodiscs were produced using the latter cooling protocol because chain incorporation into crystal plates is slow at room temperature. Since the nanodiscs are most likely kinetic products, PM packing should not be as regular as what is depicted schematically in Fig. 4b. While it would be ideal to verify this assumption about triblock chain packing shown in Fig. 4 by electron diffraction, we could unfortunately not do this for the beam damage of the particles by electrons.

3.5. Phase image change with r_{SP}

In tapping-mode AFM, the cantilever is set to oscillation by a sinusoidal driving force $F_0 \sin(\omega t)$, where ω is typically chosen to be very close to the resonance angular frequency ω_0 of the cantilever. For a free cantilever in air, the damping force is small and the steady-state cantilever oscillating amplitude is defined as A_0. The interaction between the tip and sample enhances damping and reduces the oscillating amplitude to A. The interaction also changes the phase angle ϕ between the sinusoidal driving force and the oscillating motion of the cantilever. The instrument measures ϕ as a function of position coordinates x and y of a sample and yields a phase image.

The phase images in Fig. 3 show that better phase contrast between the core and shell of the nanodiscs was obtained by increasing the tapping force, that is, by reducing r_{SP}. While such a trend has been observed in many systems which contained domains of different components, it happens here because the tip starts to differentiate between the two polymers only when the tapping force is large enough to allow the tip to penetrate through the PDMS overlayer and into the underlying PM with top surface denoted by the MM′ line in Fig. 4a.

One can differentiate polymers based on phase contrast because the phase lag $\Delta\phi$ between a free and interacting cantilever is [42,43]:

$$\Delta\phi \propto \sqrt{S}E^* \left(\frac{Q}{k}\right) \tag{1}$$

where S is the area of contact between the tip and sample; E^* is the effective Young's modulus for the tip and sample, and Q and k are the quality factor [43] and force constant for the cantilever, respectively. For polymer samples, which are normally much softer than the tip, E^* is effectively given by the Young's modulus E of the sample. Thus, AFM differentiates polymers in the phase mode due to differences in the quantity $\sqrt{S}E$.

In our system, PM and PDMS should differ in E by 4–5 orders of magnitude [41]. As the thickness of the nanodiscs is in the order of 2 nm, much smaller than the radius of curvature of 5 nm for the AFM tip, the contact area S should thus not differ significantly over the entire thickness of the polymer nanodiscs. These considerations lead us to believe that the harder PM should appear brighter over the whole r_{SP} range of interest as observed experimentally.

3.6. Topographic image change with r_{SP}

The apparent shape of the nanodiscs as probed by AFM in the topographic mode changed from discs to "donuts" and then to "filled donuts" as r_{SP} decreased. Such a topographic "height" inversion [40] has been previously observed. Tapping-mode AFM does not determine the time-average height $\langle h \rangle$ of an oscillating tip above a sample directly. Rather, it operates based on a feedback mechanism that maintains a constant oscillation amplitude A for the cantilever by adjusting $\langle h \rangle$. The topographic image deduced based on the assumption that an equal r_{SP} gives an equal $\langle h \rangle$ is correct only if there is negligible (hard materials) or comparable (the same material) tip penetration into the different regions of a sample. This assumption is generally invalid for PM and PDMS because of their drastically different hardnesses.

To explain the observed trend, we will start by examining factors that affect r_{SP}. According to classical vibration mechanic theory, the steady-state amplitude A_0 of an oscillator, which is driven in air with a damping coefficient ξ_0 by a sinusoidal force $F_0 \sin(\omega t)$ is:

$$A_0 = \frac{F_0/k}{\sqrt{\left(1 - \left(\frac{\omega^2}{\omega_0^2}\right)\right) + \left(\frac{\xi_0 \omega}{m\omega_0^2}\right)^2}} \tag{2}$$

In deriving Eq. (2), the damping force f_r is assumed to operate on the oscillator throughout the whole oscillating cycle with magnitude given by:

$$f_r = -\xi_0 v \tag{3}$$

where v is the velocity of the oscillator. Under an identical driving force, the steady-state oscillation amplitude will be reduced if the oscillator is fully immersed in a viscous liquid with a damping coefficient of ξ. The amplitude ratio A/A_0 for the two cases at ω is [43]:

$$\frac{A}{A_0} = \frac{\sqrt{\left(1-\left(\frac{\omega^2}{\omega_0^2}\right)\right)+\left(\frac{\xi_0\omega}{m\omega_0^2}\right)^2}}{\sqrt{\left(1-\left(\frac{\omega^2}{\omega_0^2}\right)\right)+\left(\frac{\xi\omega}{m\omega_0^2}\right)^2}} \tag{4}$$

In AFM, the tip may interact with a sample surface via van der Waals (i.e. attractive) forces or by repulsive forces if the tip is to penetrate it directly. Regardless of the interaction mechanism, the interaction forces are operative only through a small portion of an oscillating cycle when the tip is at its lowest point. The results of classical mechanical theories, as described by Eq. (4), thus do not apply directly. To circumvent this difficulty several different approaches have been considered [40,44]. In this study, aimed at a qualitative interpretation of our experimental results, we will simply replace ξ in Eq. (4) by an effective friction coefficient ξ_{eff}. To gain insight into the relative magnitude of ξ_{eff}, we make use of results of a numerical analysis [45] which show that for an equal $\langle h\rangle$ above a softer and a harder sample, an AFM tip penetrates the softer material further. For the longer path length of the tip in a softer matrix [45], ξ_{eff} is larger. Thus, the magnitude of ξ_{eff} increases at a given $\langle h\rangle$ as the collision between a tip and a sample becomes more sticky and less elastic.

With this background now in place, we examine next how r_{SP} varies with the apparent height $\langle h\rangle$ along the paths SS′ (the edge of the nanodisc, consisting only of soft PDMS) and CC′ (the middle of the nanodisc, consisting of harder PM, bounded on each side by a softer PDMS layer) depicted in Fig. 4a. Before the tip is able to touch the PM surface denoted by the MM′ line, the tip and sample interaction should be essentially identical along both paths. Under these conditions, AFM gives the correct topographic information, i.e. points S and C have an approximately equal height. Line AB in Fig. 5 depicts schematically how r_{SP} varies with $\langle h\rangle$ over the set point range $1.0 > r_{SP} \gtrsim 0.95$. As r_{SP} is decreased below about 0.95, the tip reaches the line MM′. A tip traveling along the path CC′ will not penetrate much beyond MM′ due to the hardness of the underlying PM. The more elastic collision between the tip and the PM layer thus leads to a less steep decline in r_{SP} with $\langle h\rangle$. In contrast, the less elastic PDMS leads to a more drastic decline in r_{SP} with $\langle h\rangle$ along the SS′ path. The variation of r_{SP} with $\langle h\rangle$ is schematically illustrated in Fig. 5 by line BF for path CC′ and line BD for path SS′. As one further

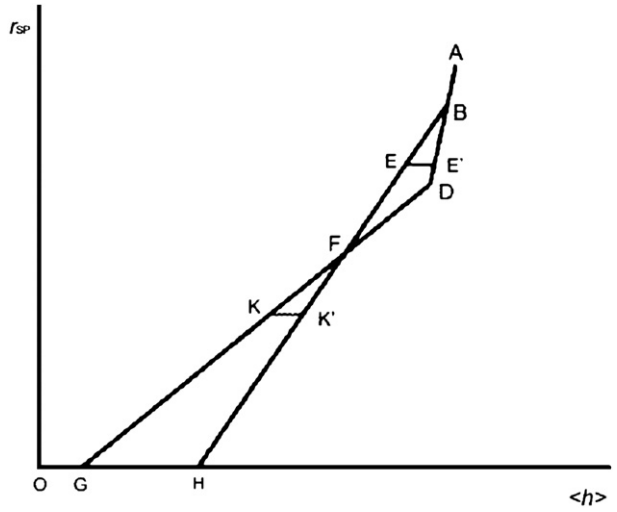

Fig. 5. Schematic illustration of how r_{SP} would change with the time-average height $\langle h\rangle$ of a tip above mica when it approaches the sample following paths SS′ and CC′ depicted in Fig. 4. For path SS′, r_{SP} decreases following lines AD and then DO. For path CC′, r_{SP} decreases following lines AB and then BH.

decreases r_{SP}, the tip reaches the mica substrate denoted by point S′ along the path SS′. Since the collision between the tip and mica is more elastic than that between the tip and PM, further decrease in $\langle h\rangle$ will lead to a less sharp drop in r_{SP} along path SS′, following the line DG in Fig. 5.

Fig. 5 clearly shows that point S (Fig. 4) should appear taller than point C in the triangular region defined by BDF in Fig. 5 when observed using tapping-mode AFM. This is best illustrated by comparing the $\langle h\rangle$ values at points E and E′, respectively. This conclusion is in agreement with the apparent donut-shaped structures that we observed experimentally at $r_{SP} \approx 0.75$ in Fig. 3. At r_{SP} values below point D in Fig. 5, the tip has penetrated completely through the PDMS layer at the margins of the nanodisc and into the underlying substrate. This leads to a contrast inversion below point F in Fig. 5 such as at points K and K′. Thus, in the triangle region defined by FGH in Fig. 5 point C in Fig. 4 appears taller than point S. This is again in agreement with the filled donut structures that we saw at $r_{SP} \approx 0.60$ in Fig. 3.

Another interesting feature about the topographic images is that the size of the nanodiscs increased with decreasing r_{SP}. This is probably due to the increased flattening of the PDMS domains with increasing tapping force. A tip can flatten a PDMS layer because it is not an infinitely thin rod but a polygon-shaped pyramid. For such a tip, its cross-sectional size increases when one moves up farther away from the tip front. Even at the very end of a tip, it has a finite size with a radius of curvature around 5 nm. Thus, the further a tip penetrates into a PDMS domain, the more it squeezes the polymer both vertically (smaller thickness) and horizontally (larger depressed area). The tip can not only flatten the PDMS phase but also feel the flatness when it hits the sample again in a neighboring site for the fast movement of the tip, i.e. at 30 kHz, and the sluggish elastic restoration of PDMS.

4. Conclusions

Cooling a toluene solution of PM-PDMS-PM from 105 °C to room temperature produced aggregates that included micrometer-sized triblock crystal plates and nanoplates or nanodiscs. The shape of the nanodiscs was established by SEM and tapping-mode AFM operating under a light tapping force or at $r_{SP} = 0.95$. Surprisingly, the nanodiscs transformed in the topographic AFM images into nanodonuts and filled nanodonuts under moderate and high tapping forces, respectively, or at $r_{SP} = 0.75$ and $r_{SP} = 0.60$. Such apparent ''height inversion'' occurred probably because the AFM tip penetrated easily into the soft PDMS domains. At $r_{SP} \approx 0.75$, the tip at its lowest points in an oscillating cycle would have penetrated the top PDMS layer and reached the top surface of a PM domain in the center of a nanodisc. Significant sample penetration after this would not have been possible due to the hardness of PM. A tip approaching from the shell region where only PDMS is present can probably undergo further polymer matrix penetration. For the more sticky collision between the tip and the sample in the latter case and thus the more efficient damping to tip oscillation, the tip would need to be further away from the surface to yield the same r_{SP} value as in the former case. Thus, the center region would appear lower. For the thinness of the nanodiscs, the tip at its lowest points in an oscillating cycle could have reached mica in the shell region as r_{SP} was further decreased to ~ 0.60. Since the collisions between the tip and mica and that between the tip and PM are both approximately elastic, one eventually obtains the correct topographic image again. Such observations may be of cautionary value to future AFM users who may jump at the glory of discovering exciting ''new morphologies'' of block copolymer aggregates.

Acknowledgment

G.L. thanks the Natural Sciences and Engineering Research Council of Canada and the Canada Research Chairs Program for financial support of this research.

References

[1] Tuzar Z, Kratochvil P. Surf Colloid Sci 1993;15:1.
[2] Forster S, Antonietti M. Adv Mater 1998;10:195.
[3] Canham PA, Lally TP, Price C, Stubbersfield RB. J Chem Soc Faraday Trans 1980;76:1857.
[4] Zhang LF, Eisenberg A. Science 1995;268:1728.
[5] Ding JF, Liu GJ, Yang ML. Polymer 1997;38:5497.
[6] Yu K, Eisenberg A. Macromolecules 1998;31:3509.
[7] Stewart S, Liu G. Angew Chem Int Ed Engl 2000;39:340.
[8] Raez J, Barjovanu R, Massey JA, Winnik MA, Manners I. Angew Chem Int Ed Engl 2000;39:3862.
[9] Frankowski DJ, Raez J, Manners I, Winnik MA, Khan SA, Spontak RJ. Langmuir 2004;20:9304.
[10] Grumelard J, Taubert A, Meier W. Chem Commun 2004;1462.
[11] Jenekhe SA, Chen XL. Science 1999;283:372.
[12] Ding JF, Liu GJ. Macromolecules 1997;30:655.
[13] Opsteen JA, Cornelissen J, van Hest JCM. Pure Appl Chem 2004;76:1309.
[14] Checot F, Lecommandoux S, Gnanou Y, Klok HA. Angew Chem Int Ed Engl 2002;41:1339.
[15] Pochan DJ, Chen ZY, Cui HG, Hales K, Qi K, Wooley KL. Science 2004;306:94.
[16] Zhu JT, Liao YG, Jiang W. Langmuir 2004;20:3809.
[17] Cameron NS, Corbierre MK, Eisenberg A. Can J Chem 1999;77:1311.
[18] Liu G, Yan X, Li Z, Zhou J, Duncan S. J Am Chem Soc 2003;125:14039.
[19] Yan X, Liu G, Li Z. J Am Chem Soc 2004;126:10059.
[20] Massey JA, Winnik MA, Manners I, Chan VZH, Ostermann JM, Enchelmaier R, et al. J Am Chem Soc 2001;123:3147.
[21] Park M, Harrison C, Chaikin PM, Register RA, Adamson DH. Science 1997;276:1401.
[22] Thurn-Albrecht T, Schotter J, Kastle CA, Emley N, Shibauchi T, Krusin-Elbaum L, et al. Science 2000;290:2126.
[23] Li Z, Zhao W, Liu Y, Rafailovich MH, Sokolov J, Khougaz K, et al. J Am Chem Soc 1996;118:10892.
[24] Silva GA, Czeisler C, Niece KL, Beniash E, Harrington DA, Kessler JA, et al. Science 2004;303:1352.
[25] Stupp SI. MRS Bull 2005;30:546.
[26] Vriezema DM, Aragones MC, Elemans J, Cornelissen J, Rowan AE, Nolte RJM. Chem Rev 2005;105:1445.
[27] Kataoka K, Harada A, Nagasaki Y. Adv Drug Deliv Rev 2001;47:113.
[28] Massey JA, Temple K, Cao L, Rharbi Y, Raez J, Winnik MA, et al. J Am Chem Soc 2000;122:11577.
[29] Cao L, Manners I, Winnik MA. Macromolecules 2002;35:8258.
[30] Stupp SI, LeBonheur V, Walker K, Li LS, Huggins KE, Keser M, et al. Science 1997;276:384.
[31] Lin EK, Gast AP. Macromolecules 1996;29:4432.
[32] Ramzi A, Prager M, Richter D, Efstratiadis V, Hadjichristidis N, Young RN, et al. Macromolecules 1997;30:7171.
[33] Kawai T, Shiozaki S, Sonoda S, Nakagawa H, Matsumot T, Maeda H. Makromol Chem 1969;128:252.
[34] Droscher M, Smith TL. Macromolecules 1982;15:442.
[35] Shea KJ, Staiger CL, Lee SY. Macromolecules 1999;32:3157.
[36] Chen ZY, Cui HG, Hales K, Li ZB, Qi K, Pochan DJ, et al. J Am Chem Soc 2005;127:8592.
[37] Hamley IW, Fairclough JPA, Ryan AJ, Bates FS, TownsAndrews E. Polymer 1996;37:4425.
[38] Weimann PA, Hajduk DA, Chu C, Chaffin KA, Brodil JC, Bates FS. J Polym Sci Part B Polym Phys 1999;37:2053.
[39] Zheng JX, Xiong HM, Chen WY, Lee KM, Van Horn RM, Quirk RP, et al. Macromolecules 2006;39:641.
[40] Bar G, Thomann Y, Brandsch R, Cantow HJ, Whangbo MH. Langmuir 1997;13:3807.
[41] Young RJ, Lovell PA. Introduction to polymers. 2nd ed. London: Chapman and Hall; 1991.
[42] Magonov SN, Elings V, Whangbo MH. Surf Sci 1997;375:L385.
[43] Steidel Jr RF. An introduction to mechanical vibrations. 3rd ed. New York: Wiley; 1989.
[44] Cleveland JP, Anczykowski B, Schmid AE, Elings VB. Appl Phys Lett 1998;72:2613.
[45] Sarid D, Ruskell TG, Workman RK, Chen D. J Vac Sci Technol B 1996;14:864.